VDW

The average relative arrangements and movement of molecules within a liquid are primarily determined by local packing and steric effects from short-range repulsive intermolecular forces. The range of forces (attractive, dipole-dipole, other slow varying interactions) play a minor role in the structure and provide a simple approximation of a mean field (spatially uniform background potential) that exerts no intermolecular force and has no effect on the structure or dynamics but provides the cohesive energy making the system stable at a certain density and pressure. Attractive intermolecular interactions have no effect on the structure. VDW attractions often arise from electrostatic effects such as fluctuating dipole-induced dipole interactions (dispersion interactions). These forces are not associated with significant distortions of intramolecular charge distributions; thus their magnitudes are not often large. Spatial variations of attractive interactions are around $k_B T_T$ per one molecule diameter, k_B being Boltzmann's constant and T_T is the triple point temperature of the material. Short range repulsions are around $k_B T_T$ per 1/10 of an atomic/molecular diameter.

The intermolecular force is given by the gradient potential $-dw(r)/dr,$ thus particles repel each other at separations less than the potential minimum at $r_0 = 2^{1/6}\sigma$ with σ being a length scale parameter. The change in energy associated with any local (short wavelength) displacement will be dominated by interparticle repulsive forces. Attractive forces are much weaker an cancel each other out, leaving only averaged uniform background energy. The WCA theory of liquids towards short- and long-range forces explains the radial distribution function of repulsive forces depending on the potential $u_0(r)$ through the Boltzmann factor (exp $[-\frac{u_0(r)}{k_B T}]$). This ranges from 0 to 1 over a small range of r values, while the Boltzmann factor for the hard sphere potential (exp $[-u_d(r)/k_B T]$) which is a step function that changes from 0 to 1 at exactly r = d. The Boltzmann factor describes the effect of direct interaction between a pair of particles separated by a distance r. In a liquid, correlations between that pair of particles are affected by all the surrounding particles.

In Barker-Henderson theory (BH), the potential $w(r)$ is divided into positive ($r < \sigma$) and negative ($r > \sigma$) parts. Close proximity of neighboring particles in a dense liquid allows the background uniform energy to rescale from zero to the potential minimum at r_0 where the force changes from repulsive to attractive. However, BH leaves out the repulsive forces between σ and r_0 and underestimates the size of particles, being the most important structural parameter in VDW. The accuracy of VDW depends on a clear separation of the intermolecular potential into a short range harshly repulsive portion and a longer range (generally attractive) part which is a relatively slow varying function. Problems in understanding VDW materials is the determination of entropic effects of packing.

[Chandler, D., Weeks, J.D. and Andersen, H.C., 1983. Van der Waals picture of liquids, solids, and phase transformations. *Science*, *220*(4599), pp.787-794.]

VDW force are always present and contribute to all measurements. Resulting VDW forces can be represented as a volume integral of the atomic intermolecular forces as derived by Hamaker, simplified for small separations $d \ll R$:

$$F_{TS}(z_c, z) = -\frac{HR}{6d^2}$$

where $d = z_c + z$, and H is the Hamaker constant, R is tip radius, z_c the rest tip-surface separation, z the instantaneous tip position, and d is the instantaneous tip-surface distance. In the contact region the force is taken as:

$$F_{TS}(DMT, d) = F_{TS,a}(a_0) + \frac{4}{3}E^*\sqrt{R(a_0 - d)^3}, \qquad d < a_0$$

where the first term on the RHS is the adhesion force and the last term is the repulsive force by DMT theory. a_0 is an intermolecular distance used to avoid divergence and implies contact occurs at cantilever separation a_0.

Phase

The resonant frequency (w_r is the angular resonant frequency of the free air cantilever) and natural frequency (w_0 natural frequency of cantilever) are related by:

$$w_r = w_0(1 - \frac{1}{2Q^2})^{1/2}$$

where large enough values for Q (air or UHV) that $w_r \approx w_0$.

$$\langle E_{dis}\rangle_{CYCLE} = \frac{\pi k A_0 A_{SP}}{Q}\left[SIN(\phi) - \frac{A_{SP}}{A_0}\right], \qquad w = w_0$$

Any background damping such as air damping and the viscosity involved in the internal beam damping is not included in the expression $\langle E_{dis}\rangle$ and it does not impose any restriction on the tip-sample force. Nevertheless, since a harmonic response is assumed to derive it, when the excitation of higher harmonics in the interaction is relevant, this expression cannot be used reliably. Thus, can be safely used in air but typically not in liquid for softer cantilevers where harmonics need to be accounted for. Taking this into account and looking at it is easy to observe that the first term inside the brackets, the sin of the phase, is dissipative while, the second term, $\frac{A_{SP}}{A_0}$, is conservative.

[Hernandez, S.S., 2011. *Dynamic Atomic Force Microscopy and applications in biomolecular imaging*. University of Leeds.]

AFM operated with amplitude modulation feedback has two regimes of operation, attractive and repulsive. In the first regime, a net attractive force dominates the amplitude reduction while in the other a net repulsive force controls the cantilever dynamics. The operating regime is attractive when the average force in one oscillation is negative. In most situations, the amplitude decreases with the tip-sample proximity. However, a sharp jump in the amplitude curves has been reported. This jump has been attributed to the onset of the repulsive regime, i.e., the oscillation switches from a purely noncontact (long-range attractive forces) to tapping mode (attractive and repulsive). However, we find that a step-like discontinuity in the amplitude curve is not an exclusive characteristic of the noncontact to intermittent contact transition. We show that a discontinuity is always a consequence of the existence of two oscillation states.

[Garcia, R. and San Paulo, A., 1999. Attractive and repulsive tip-sample interaction regimes in tapping-mode atomic force microscopy. *Physical Review B, 60*(7), p.4961]

VDW forces at nanostructures

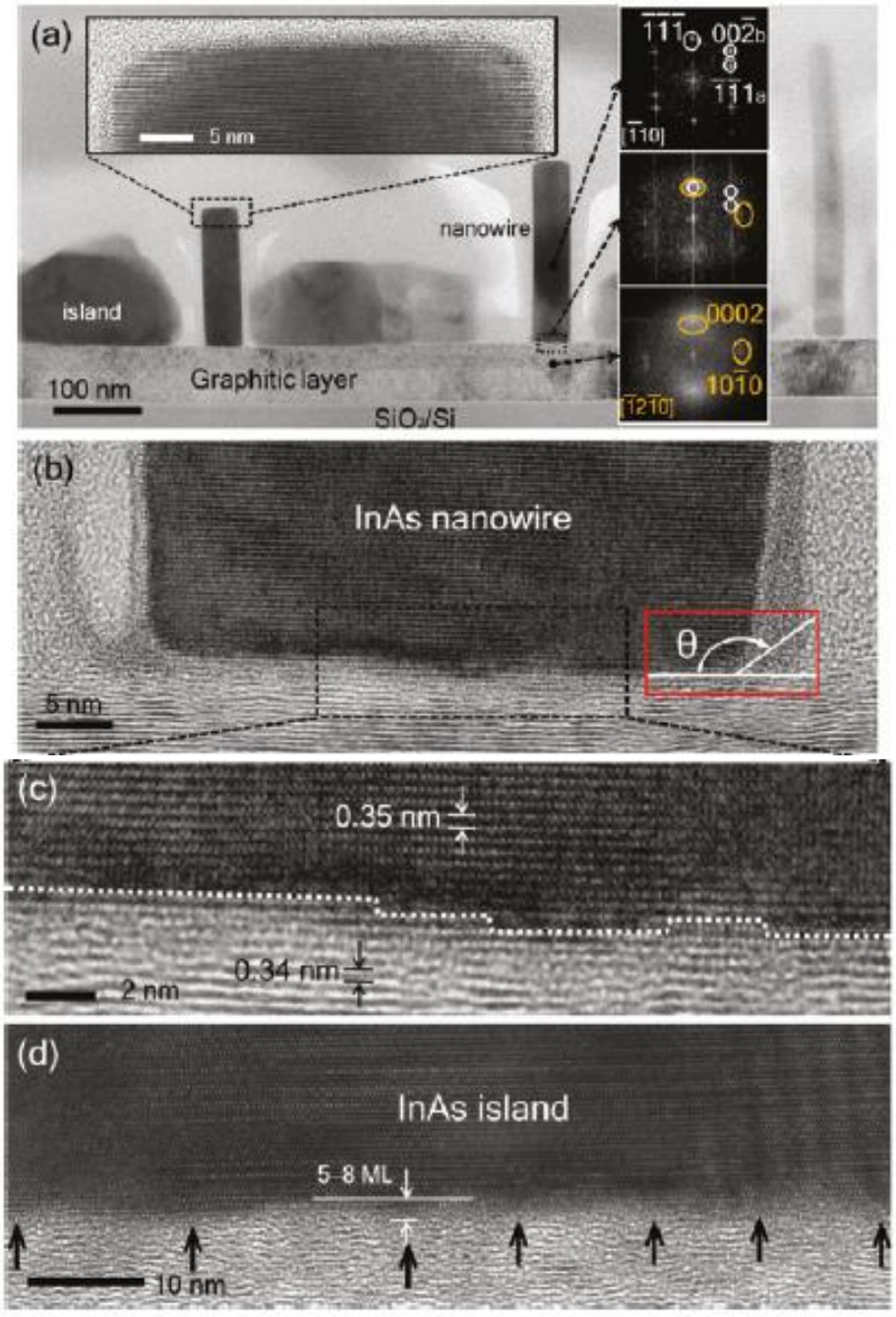

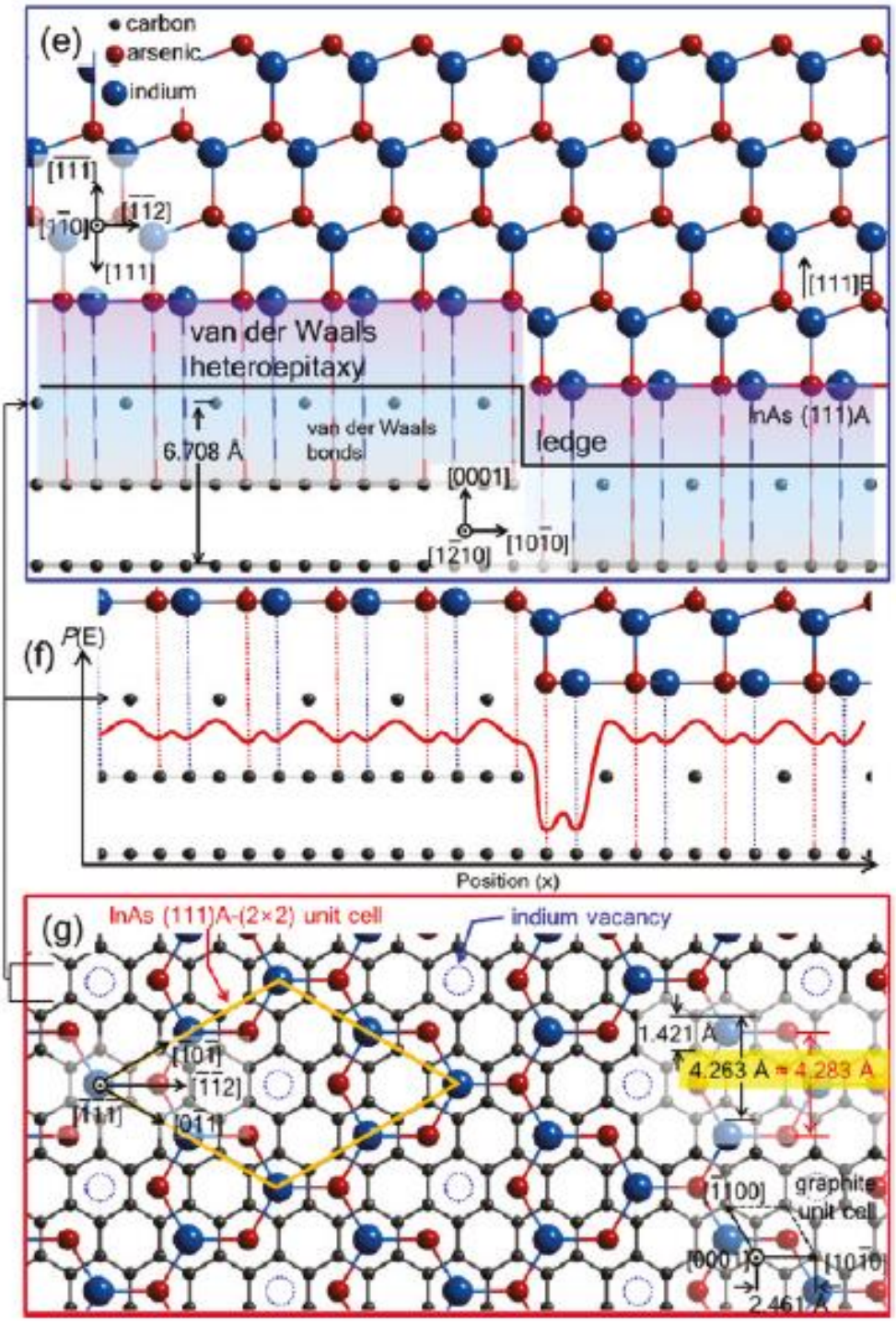

Figure 1: VDW heteroepitaxy of InAs nanowires on honeycomb carbon surface. (a) Cross-sectional TEM image of InAs nanowires and islands grown on graphitic films. Left inset in (a) is the TEM image taken around the nanowire tip showing the flat top surface. Right insets in (a) are the selected area diffraction patterns of the InAs nanowire (top panel), the interface of InAs and graphitic layer (middle panel), and the graphitic layer (bottom panel), obtained through the FFT process. (b) TEM image showing the interface of InAs nanowire and graphitic layers. The red box in (b) exhibits an obtuse contact angle between InAs and graphitic layer, implying the nonwetting graphitic surface. (c) High-resolution TEM image of the enclosed area in (b), showing the 1-2 ML ledges of graphitic layer are underneath the nanowire bottom. These ML ledges provide the heterogeneous nucleation site for the nanowire growth. The lattice spacings between adjacent planes in the nanowire and graphitic layer

regions were measured to be 0.35 and 0.34 nm, corresponding to the d spacings of InAs (111) and graphite (0002) planes, respectively. (d) TEM image showing the interface of InAs island and graphitic layers. The arrows in (d) present very rough graphitic surface with high-density ledge grooves. (e-g) Schematic representations of the atomic configuration model for the VDW heteroepitaxy of InAs nanowires on carbon honeycomb lattices. (e) Schematic viewed along the InAs ($\bar{1}10$) zone axis. (f) Schematic plot of the potential energy for the van der Waals heteroepitaxy of InAs on graphitic layers as a function of position on the graphitic surface. (g) Atomic configuration model showing how indium and arsenic atoms occupy their positions on the honeycomb carbon surface for the van der Waals heteroepitaxy

However, the ledges or kinks still offer deep potential wells owing to their infinitesimal radius of curvature, as forces. The maximized cohesive force enables the heteroepitaxial formation of vertical nanowire morphology, even though the VDW bonding energy is much smaller than that of covalent bond (typically a few electron-volts) by 2 or 3 orders of magnitude.

[Hong, Y.J. and Fukui, T., 2011. Controlled van der Waals heteroepitaxy of InAs nanowires on carbon honeycomb lattices. *ACS nano*, *5*(9), pp.7576-7584.]

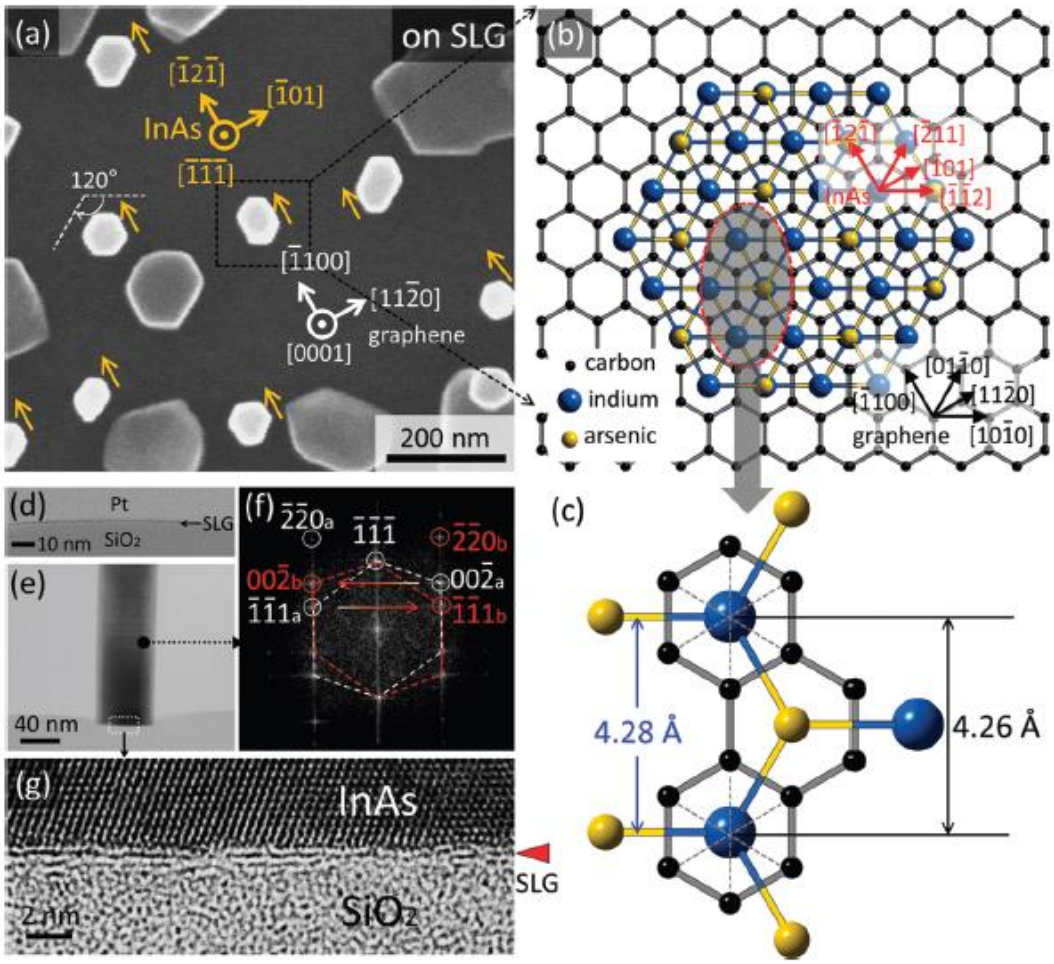

Figure : Vertically well-aligned InAs nanowires heteroepitaxially grown on SLG. (a) Top-view FE SEM image of InAs nanowires grown heteroepitaxially on SLG films. Brighter structures are nanowires with a hexagonal prismatic shape. (b-c) Schematic images of the atomic configuration

presenting the nearly coherent heteroepitaxial relationship of zinc blende InAs-$(\overline{1}\overline{1}\overline{1})[\bar{1}10]$||SLG-$(0001)[1\bar{2}10]$. (d) Cross-sectional TEM image of SLG film transferred onto a SiO2/Si substrate. (e) Low-magnification cross-sectional TEM image of InAs nanowire vertically grown on SLG. (f) Selected-area diffraction pattern obtained through a FFT process of the HR-TEM image of nanowire. (g) HR-TEM image of the enclosed area in (e), showing the interface of InAs/SLG/SiO2.

Electrical van der Waals force interactions arise from permanent dipole–permanent dipole interactions (the orientation effect – Keesom forces), permanent dipole–induced dipole interactions (the induction effect – Debye forces), and/or induced dipole–induced dipole interactions (the dispersion effect – London forces). The structure of molecular solids is fundamental to understand these interactions which include general features of the electronic structure of atoms, i.e., the arrangement of electron clouds around the central nucleus. In particular, the London dispersion forces generated by electron movements in the interacting molecules usually are the biggest contribution to VDW interactions. Also, it is known that this effect acts on non-polar molecules like hydrocarbons, and their magnitude depends on the polarizability (electron density with the capacity for an induced dipole). Although the VDW forces are weak when compared to covalent and ionic chemical bonds, their cooperative action in practical terms is capable of reaching orders of magnitude that can be perceived on the macroscale as, for instance, the adhesive interaction of the gecko's foot on walls and ceilings.

[Echeverrigaray, F.G., de Mello, S.R., Leidens, L.M., da Costa, M.E.M., Alvarez, F., Burgo, T.A., Michels, A.F. and Figueroa, C.A., 2018. Towards superlubricity in nanostructured surfaces: the role of van der Waals forces. *Physical Chemistry Chemical Physics*, *20*(34), pp.21949-21959.]

Though DVLO theory, which assumes that the separation between particles is controlled by the balance between Coulombic and van der Waals forces, is often employed to describe the total interaction potential between microscopic objects, its applicability to nanoscale entities has yet to be established.

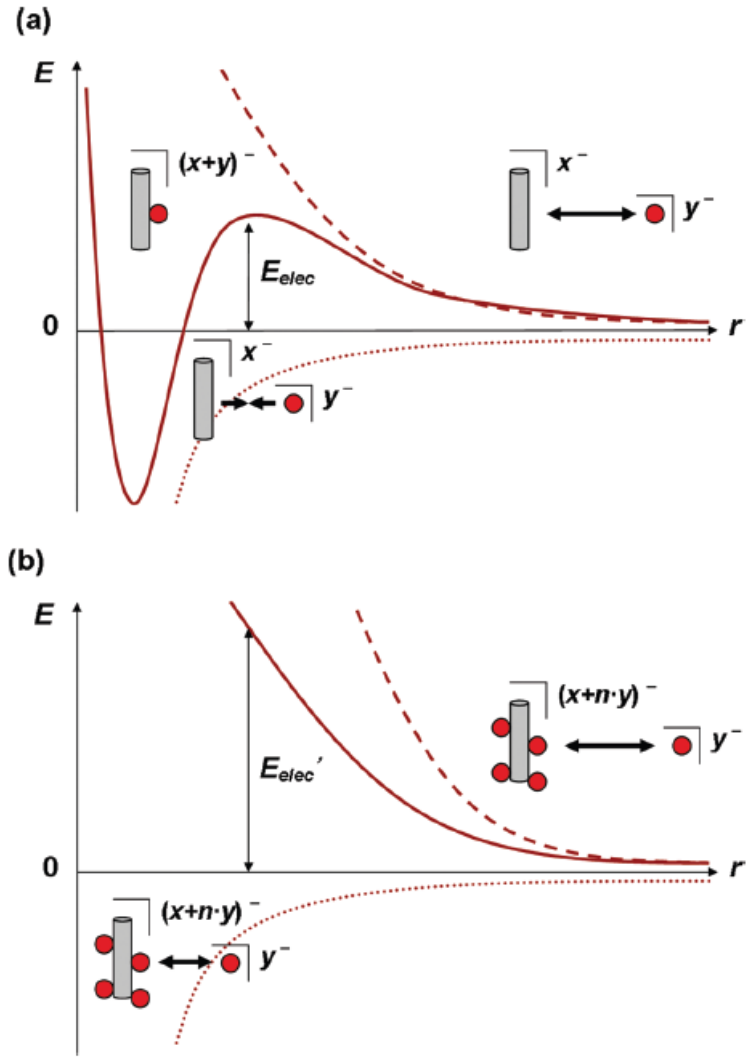

Figure : Schematic representation of the relative energies of the repulsive Coulombic (dashed line) and attractive van der Waals (dotted line) forces as a function of distance between negatively charged nanoparticles and negatively charged nanotubes. (a) Initially, nanoparticles have to overcome the barrier E_{elec} provided by electrostatic repulsion of x^- and y^- surface charges on MWNTs and AuNPs, respectively. (b) As more nanoparticles adsorb on nanotubes, the electrostatic repulsion increases ($E_{elec}' > E_{elec}$) eventually halting the adsorption process. The arrows reflect the sign and magnitude of the interactions between the two nanoscopic species. Surface functional groups have been omitted for clarity. VDW interactions with other nanoscale and molecular species are likely to be much more long-range (~$1/r^3$) than those typically observed between colloidal species (~$1/r^6$).

[Rance, G.A., Marsh, D.H., Bourne, S.J., Reade, T.J. and Khlobystov, A.N., 2010. van der Waals interactions between nanotubes and nanoparticles for controlled assembly of composite nanostructures. *ACS nano*, *4*(8), pp.4920-4928.]

The double-layer electrostatic $U = U\text{vdW} + U\text{dl} + U\text{h}$ is divided it into the van der Waals, double-layer electrostatic, and hydration parts.

[Zhdanov, V.P., 2017. Nanoparticles in a nanochannel: Van der Waals interaction and diffusion. *Physics Letters A*, *381*(34), pp.2832-2836.]

The approach used to develop this model is analogous to that used in Derjaguin Landau Verwey Overbeek (DLVO) theory for colloidal stability. Specifically, it is assumed that the contributions to the total interaction energy are additive. These contributions come from charge transfer attraction, van der Waals attraction, osmotic repulsion, elastic repulsion and non-elastic repulsion. It was found that Derjaguin approximation is unsuitable for systems where the radius of curvature of the surface is comparable with the range of interactions.

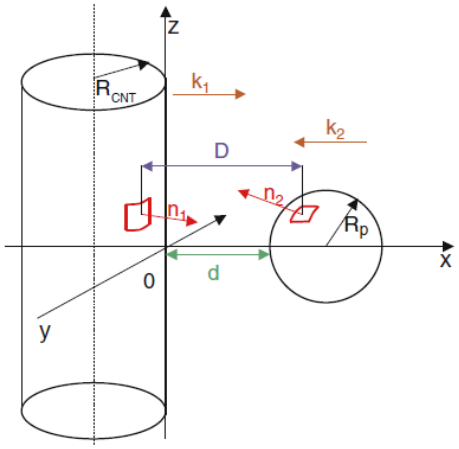

Figure : Illustration of the interaction between a MWCNT and a nanoparticle, represented as a cylinder and a sphere, respectively.

[Stolarczyk, J.K., Sainsbury, T. and Fitzmaurice, D., 2007. Evaluation of interactions between functionalised multi-walled carbon nanotubes and ligand-stabilised gold nanoparticles using surface element integration. *Journal of computer-aided materials design*, *14*(1), pp.151-165.]

There are two methods for calculating the VDW energy between macroscopic bodies. One is the microscopic theory developed by Hamaker, and the other is the macroscopic theory developed by Lifshitz. The London dispersion forces are attractive, acting between two electric dipoles induced by asymmetric fluctuations of orbiting electrons of atoms, and are proportional to r^{-7}, where r is the separation between the atoms. When r becomes so large that the propagation time of the induced dipole field of atom 1 to and from atom 2 is not negligible compared to the fluctuating period of the dipole, the r dependence of the VDW energy changes asymptotically from r^{-7} (non-retardation) to r^{-8} (retardation). This was confirmed experimentally.

2 are denoted by dx, dy, and dz, respectively, which are shown with short blue lines in Figure 1. The length, thickness, and width of the bodies are denoted by $2L$, $2t$, and $2w$ respectively, and suffix 1 or 2 is the body number.

Generally, the London–vdW interaction energy between a pair of macroscopic bodies, V_R, in the nonretardation region is given by Hamaker[16]

$$V = -(A/\pi^2)V_R$$

$$V_R = \iint_{v_1,v_2} (1/r^6)\mathrm{d}v_1\, \mathrm{d}v_2 \tag{1}$$

where A is the Hamaker constant, $r^2 = (x_2 - x_1)^2 + (y_2 - y_1)^2 + (z_2 - z_1)^2$, $dv_1 = dx_1\, dy_1\, dz_1$, and $dv_2 = dx_2\, dy_2\, dz_2$, where x_1, y_1, and z_1 are the x, y, and z coordinates of an arbitrary point in body 1 and x_2, y_2, and z_2 are those in body 2.

The integrations are simply conducted over the volume of the respective bodies, v_1 and v_2. Using $x = x_2 - x_1$, $y = y_2 - y_1$, and $z = z_2 - z_1$, the six integrations in eq 1 are carried out in the order $(z, z_1) \rightarrow (y, y_1) \rightarrow (x, x_1)$ as follows

$$\begin{aligned}
V_R(dx, dy, dz) &= \int_0^{2w_1} \int_{2w_1+dx-x_1}^{2w_1+2w_2+dx-x_1} dx_1\, dx \\
&\quad \int_0^{2t_1} \int_{2t_1+dx-y_1}^{2t_1+2t_2+dy-y_1} dy_1\, dy \times \{V_z(x, y, dz + 2L_1 + 2L_2) \\
&\quad + V_z(x, y, dz) - V_z(x, y, dz + 2L_1) - V_z(x, y, dz + 2L_2)\} \\
&= \int_0^{2w_1} \int_{2w_1+dx-x_1}^{2w_1+2w_2+dx-x_1} dx_1\, dx \int_0^{2t_1} \int_{2t_1+dy-y_1}^{2t_1+2t_2+dy-y_1} dy_1\, dy \\
&\quad \sum_{i=1}^{4} (-1)^i V_x(x, y, a_i) \\
&= \int_0^{2w_1} \int_{2w_1+dx-x_1}^{2w_1+2w_2+dx-x_1} dx_1\, dx \sum_{j=1}^{4} \sum_{j=1}^{4} (-1)^{i+j} V_{xy}(x, b_j, a_i)
\end{aligned}$$

By substituting a_i, b_j, and c_k $(i, j, k = 1, 4)$ in eq 3 into V_{xyz} in eq 2, the final form of V_R is obtained as follows,

$$V_R(dx, dy, dz) = \sum_{k=1}^{4}\sum_{j=1}^{4}\sum_{i=1}^{4}(-1)^{i+j+k}$$

$$\left[\left\{\frac{c_k(a_i^2 + b_j^2)^{3/2}}{24a_i^2b_j^2}\right\}\tan^{-1}\left(\frac{c_k}{\sqrt{a_i^2 + b_j^2}}\right)\right.$$

$$+\left(\frac{3}{32}\right)\left(\frac{c_k}{b_j} - \frac{b_j}{c_k}\right)\tan^{-1}\left(\frac{b_j}{c_k}\right)$$

$$+\left(\frac{1}{24}\right)b_j\left(\frac{1}{a_i^2} + \frac{1}{c_k^2}\right)\sqrt{a_i^2 + c_k^2}\tan^{-1}\left(\frac{b_j}{\sqrt{a_i^2 + c_k^2}}\right)$$

$$+\left(\frac{1}{24}\right)a_i\left(\frac{1}{b_j^2} + \frac{1}{c_k^2}\right)\sqrt{b_j^2 + c_k^2}\tan^{-1}\left(\frac{a_i}{\sqrt{b_j^2 + c_k^2}}\right)$$

$$\left.\left(\frac{1}{32}\right)\log\left\{\frac{(b_j^2 + c_k^2)^3}{c_k^2(a_i^2 + b_j^2 + c_k^2)^2}\right\}\right] \qquad (5)$$

This equation (V_R) diverges at $a_i = 0$ or $b_j = 0$; in these cases, V_R is partially modified as shown in the Appendix section.

[Maeda, H. and Maeda, Y., 2015. Orientation-Dependent London–van der Waals Interaction Energy between Macroscopic Bodies. *Langmuir*, *31*(26), pp.7251-7263.]

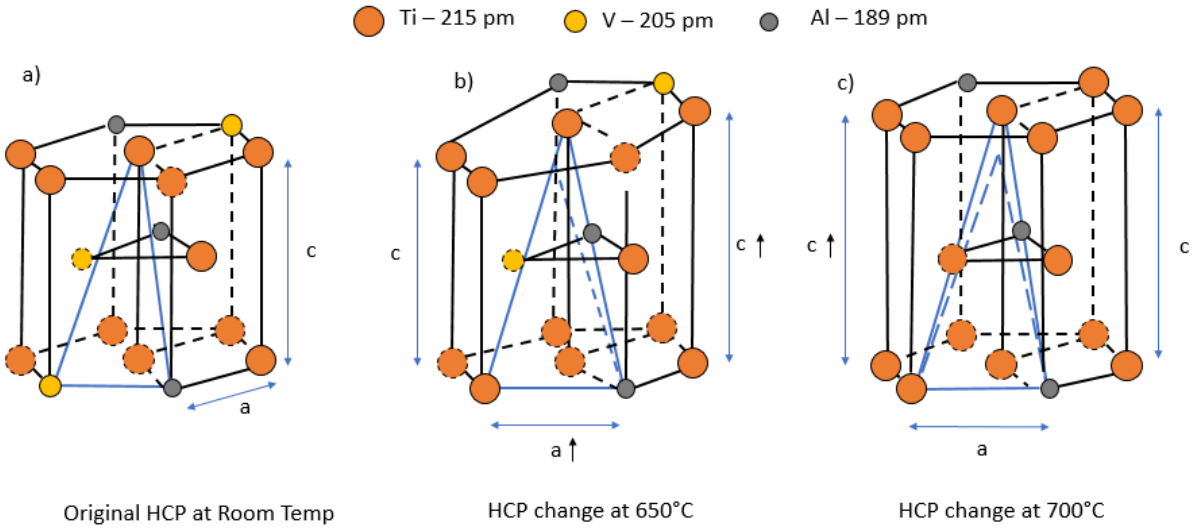

Figure : Schematic of lattice parameter change with increased heating of additively manufactured specimen. a) illustrates the original HCP crystal structure at 23 °C; b) depicts a skewed HCP structure due to the expansion of the basal plane and one prismatic plane due to the expulsion of vanadium

during heating at 650 °C; c) shows an expanded HCP lattice structure upon heating at 700 °C with equal prismatic planes due to further expulsion of vanadium atoms.

The Figure above illustrates a schematic of the lattice expansion due to heating of the lamellae specimen. In the schematic of the HCP crystal with hypothetical composition of Ti-6Al-4V is illustrated with titanium (Ti) in orange, vanadium (V) in yellow and aluminium (Al) in grey. In the results it was observed that upon heating the lattice parameter increases. This increase may be due to the expulsion of V atom from the basal plane during heating of the alloy. The expulsion of such atom of atomic size 205 pm causes a Ti atom to take its place (atomic size 215 pm). As a result, a greater atomic repulsive force now exists between atoms within the HCP structure causing it to change, producing a crystal structure which is distorted. Upon further heating, another V atom appears to be expelled and replaced by a Ti atom allowing the HCP to accommodate, and return on a stable, equilibrium lattice structure with balanced repulsive forces.

[Kaschel, F.R., In-process and Post-process Characterisation of Additively Manufactured Ti-6Al-4V Parts.

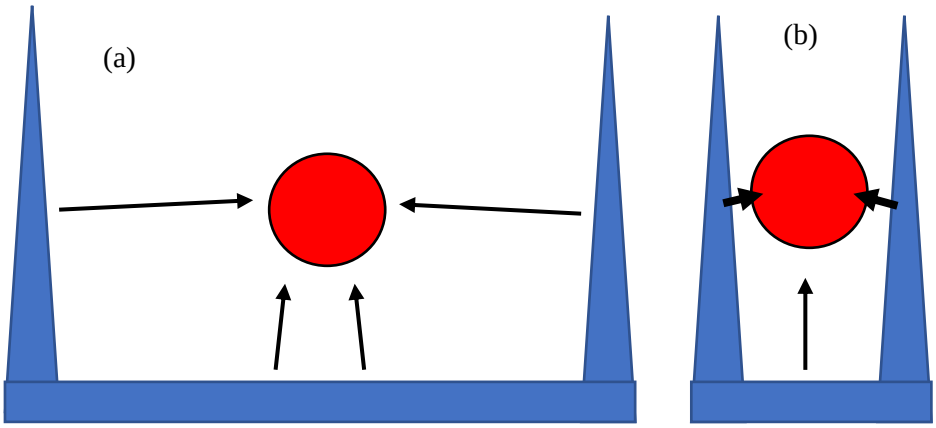

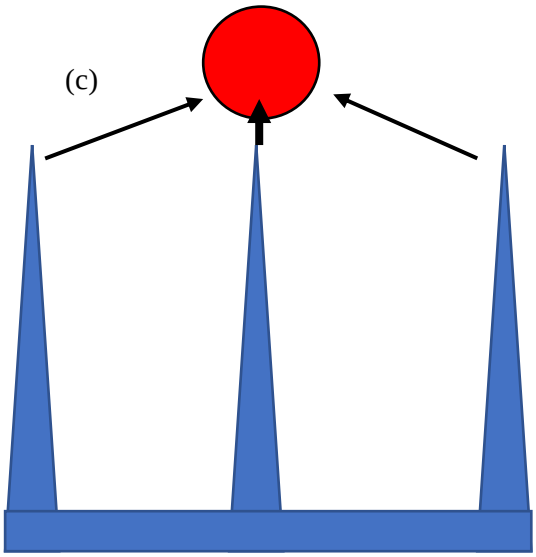

Figure : Forces (VDW) experienced generally on a spherical particle such as a cell by vertical nanostructures. (a) The cell is within a widely-spaced NS array and experiences relatively even (depending on absolute position) forces, (b) narrow-spaced NS array, as the narrower the spacing relative to the cell, greater forces from the side-wall occur than from the base, and (c) as the cell lands on top of a NS or NSs there is a maximal force from the 'contacting' NS(s) with smaller contributions from neighbouring NS.

Adhesion papers

Macrophages play an important role in immune response and tissue homeostasis. The ability of macrophages to perform phagocytosis renders them effective at killing microbes and clearing apoptotic and necrotic cells. The hallmarks of macrophage activation can be verified by cell adhesion and spreading on the extracellular matrix (ECM). Among the ECM components, fibronectin (F_n) has been recognized as the key element promoting cell adhesion, among its other functions. Adhesion to F_n modulates the secretion of proinflammatory cytokines and contributes to cell migration through various tissues. These functions are mediated by surface receptors, called integrins, which are present on macrophages. The migratory process involves a repeated, dynamic deformation and recovery of the plasma membrane; however, it is not yet fully understood whether this capacity for deformation is influenced by cell adhesion to the ECM. The tension in the plasma membrane generates inward forces that influence all the cellular processes involving membrane deformations. The apparent membrane tension in cells is a sum of the in-plane tension in the bilayer and the adhesion energy between the membrane and the Cytoskeleton. Thus, there is great interest in investigating the membrane cytoskeleton adhesion, which can vary among different cell types. However, even though there is a close association between the cell membrane and the cytoskeleton, there is still a lack for information about the impact of the ECM on the elastic modulus of the plasma membrane. Currently, It is important to note that the measurements performed around the nucleus, where the cells were thicker (more than 4 μm), were less prone to artifacts because of the hardness of the substrate.

For cells cultured on an uncoated substrate, the RMS value was 86.5 nm, whereas for cells cultured on an F_n-coated substrate, it was 100.2 nm. Therefore, the roughness analysis showed that cells cultured on coated substrates have a higher RMS (higher roughness) than those cultured on uncoated substrates. In macrophages plated on an uncoated substrate (control), the average Young´s moduli were 48.5 ± 7.3 and 47.7 ± 7.2 kPa (mean ± SD). The average Young's moduli of macrophages adhered to F_n-coated substrates were 63.9 ± 11.3 kPa and 71.1 ± 10.4 kPa (mean ± SD). The F_n affected the elasticity of macrophages, causing a 32 % increase in the average Young's modulus after 1 h and 49 % after 48 h as compared with uncoated control substrates.

[Souza, S.T., Agra, L.C., Santos, C.E., Barreto, E., Hickmann, J.M. and Fonseca, E.J., 2014. Macrophage adhesion on fibronectin evokes an increase in the elastic property of the cell membrane and cytoskeleton: an atomic force microscopy study. *European Biophysics Journal*, *43*(12), pp.573-579.]

Measurements of cell stiffness have therefore been essential for determining the biomechanical effects of various drugs and treatments relevant to cells in circulation.

[MacQueen, L.A., Buschmann, M.D. and Wertheimer, M.R., 2010. Mechanical properties of mammalian cells in suspension measured by electro-deformation. *Journal of Micromechanics and Microengineering*, *20*(6), p.065007.]

Data suggests that for spherical indenters we can correctly infer the geometry of contact between cell and tip solely from knowledge of the sphere radius and the depth of indentation. This suggested that even for forces routinely utilized for elasticity measurements (1–10 nN), the contact area between the cell and the cantilever can have contributions both from the pyramidal tip and from the cantilever underside.

[Harris, A.R. and Charras, G.T., 2011. Experimental validation of atomic force microscopy-based cell elasticity measurements. *Nanotechnology*, *22*(34), p.345102.]

Table 1
Tip–surface adhesion forces on cell surface, at cell–cell interface and at cell–substratum periphery (mean±S.D.)

Time (h)	Bacteria surface (nN)	Cell–substratum periphery (nN)	Cel (nN
1	−4.07±0.40	−5.08±0.40	n/a
2	−4.08±0.47	−5.37±0.60	n/a
4	−4.25±0.39	−5.88±0.70	n/a
8	−4.10±0.31	n/a	–
12	−3.87±0.74	n/a	–
36	−3.96±0.39	n/a	–

[a] n/a: not applicable.